Theory of two-photon entanglement in type-II optical parametric down-conversion

Morton H. Rubin, David N. Klyshko,* Y. H. Shih, and A. V. Sergienko
Department of Physics, University of Maryland–Baltimore County, Baltimore, Maryland 21228-5398
(Received 2 March 1994)

The theory of the two-photon state generated by type-II optical parametric down-conversion is studied with emphasis on the space-time and polarization entanglement of the photons. Several experiments are reviewed that demonstrate various aspects of the quantum nature of this state. The theory of a different type of two-photon interferometer is presented.

PACS number(s): 42.50.Dv, 03.65.Bz, 42.65.Ky

I. INTRODUCTION

The study of the foundations of quantum mechanics has recently attracted a great deal of attention because of the development of experimental techniques to generate quantum states of a particularly interesting kind called completely entangled or Einstein-Podolsky-Rosen (EPR) states. Entangled states are states of two or more particles that cannot be written as products of single-particle states. EPR states are two-particle entangled states such that the measurement of an observable of either particle determines the value of that observable for the other particle with unit probability. The importance of these states has been known since the earliest days of quantum theory [1–3]. They play a particularly important role in the study of the Einstein-Podolsky-Rosen paradox and in the study of Bell inequalities [4,5].

A powerful tool for generating these states is optical parametric down-conversion (OPDC). In OPDC, a beam of radiation, called the pump, is incident on a birefringent crystal. The pump is intense enough so that nonlinear effects lead to the conversion of pump photons into pairs of correlated photons. The down-conversion is said to be of type I or type II, depending on whether the photons in the pair have parallel or orthogonal polarization. The photons in a pair may come out in different directions or they may come out in the same direction (collinearly). The frequency and direction of the photons is determined by the orientation of the crystal.

OPDC has been studied for many years [6–13]. In this paper we shall review collinear type-II OPDC, paying particular attention to both the space-time and spectral nature of the two-photon state and the nature of its entanglement. We will then consider the passage of the beams through linear optical devices and the detection of the photons. This will lead us to a review of the recent experiments performed using collinear type-II OPDC.

These experiments are especially interesting in that they illustrate the production of entangled states that show the entanglement of spin and space-time variables. One example of the experimental consequence of this is demonstrated in the beating experiment discussed in Sec. V C. Another consequence of this is presented in Sec. V D, where a different type of second-order interferometer is discussed in which spatial interference with 100% visibility and period of the pump wavelength occurs.

II. THE EFFECTIVE HAMILTONIAN AND THE STATE VECTOR

In the interaction picture the effective Hamiltonian for the optical parametric process of type II in a crystal pumped by a laser beam is

$$H_1=\varepsilon_0\int_V d^3r\,\chi E_p^{(+)}E_o^{(-)}E_e^{(-)}+\text{H.c.}\ , \tag{1}$$

where V is the volume of the crystal illuminated by the pump laser E_p, χ is the nonlinear electric susceptibility tensor, and H.c. means the Hermitian conjugate. The polarization of the electric field E_o corresponds to an ordinary ray and E_e to an extraordinary ray in the birefringent crystal. The electric fields of the output beams for polarization $j=o,e$ are given by the quantized fields

$$E_j^{(+)}=\sum_{\mathbf{k}}E_{j\mathbf{k}}a_{j\mathbf{k}}e^{i(\mathbf{k}\cdot\mathbf{r}-\omega_{j\mathbf{k}}t)}\ , \tag{2}$$

where $a_{j\mathbf{k}}$ is the annihilation operator for the mode with polarization j and wave number $\mathbf{k}$. The dispersion relation inside the crystal is $|\mathbf{k}|=\omega_{j\mathbf{k}}n_{j\mathbf{k}}/c$, $n_{j\mathbf{k}}$ is the index of refraction,

$$E_{j\mathbf{k}}=i\left[\frac{\hbar\omega_{j\mathbf{k}}}{2\varepsilon_0 n_{j\mathbf{k}}^2V_Q}\right]^{1/2}\ , \tag{3}$$

and V_Q is the quantization volume. The creation and annihilation operators are normalized so that

$$[a_{j\mathbf{k}},a_{m\mathbf{q}}^{\dagger}]=\delta_{jm}\delta_{\mathbf{kq}}\ . \tag{4}$$

The pump field is assumed to be a classical plane wave

$$E_p^{(+)}=E_0e^{i(k_pz-\omega_pt)} \tag{5}$$

*Permanent address: Quantum Radiophysics Division, Department of Physics, Moscow State University, Moscow 119899, Russia.

and $E^{(-)}$ is the Hermitian conjugate of quantum field operator $E^{(+)}$. The z direction is assumed to be parallel to the pump beam and perpendicular to two of the faces of the crystal. The Hamiltonian (1) can be derived from the standard minimum coupling Hamiltonian for the electromagnetic field interacting with a crystal under the assumption that the wavelength of the electromagnetic radiation is much longer than the size of the molecules that compose the crystal. In writing this form of the Hamiltonian we ignore the reflections from the crystal surfaces and we make the rotating-wave approximation [6].

In Appendix A we calculate the state vector to first order in the interaction, making the assumption that the pump field is turned on adiabatically and that a steady state is attained. To simplify the computations, we make the additional assumptions that the cross section of the laser beam is constant and large enough so that diffraction effects can be ignored.

In the experiments to be discussed the crystal was oriented so that the output beams were collinear with the pump. In this case, we ignore the components of the wave vectors perpendicular to the pump beam and write $\mathbf{k}=k\hat{\mathbf{e}}_z$, $\mathbf{k}'=k'\hat{\mathbf{e}}_z$, $\hat{\mathbf{e}}_o=\hat{\mathbf{e}}_x$, and $\hat{\mathbf{e}}_e=\hat{\mathbf{e}}_y$. We drop the vector notation for the wave vectors. In this simplified case, the wave function at the output surface of the crystal may be written as a superposition of the vacuum and a two-photon state

$$|\Psi\rangle=|0\rangle+\sum_{k,k'}F_{kk'}a_{xk}^{\dagger}a_{yk'}^{\dagger}|0\rangle\ . \tag{6}$$

The coefficient $F_{kk'}$ is given by

$$F_{kk'}=g(\omega_{ok})\delta(\omega_{ok}+\omega_{ek'}-\omega_p)h(L\Delta_{kk'})\ , \tag{7}$$

where $g(\omega_{ok})=\Gamma_{kk'}L$ and $\Gamma_{kk'}$ is defined in Appendix A and is called the parametric gain index for perfect phase matching. The only fact that we need to know about g is that it is sufficiently slowly varying over the bandwidth of the down-conversion process that it may be taken as a constant. The time integral gives $2\pi\delta(\omega_{ok}+\omega_{ek'}-\omega_p)$, which is the steady-state or frequency phase-matching condition, and the integral over the length L of the crystal is $Lh(L\Delta_{kk'})$, where

$$h(x)=\frac{1-e^{-ix}}{ix} \tag{8}$$

and $\Delta_{kk'}=k_p-k-k'$. $h(L\Delta_{kk'})$ determines the natural spectral width of the two-photon state, as we shall see. If L is infinite, then the integral over the length of the crystal becomes a δ function. In this case the conditions

$$\omega_{ok}+\omega_{ek'}=\omega_p\ ,\quad k+k'=k_p \tag{9}$$

both hold and the phase matching is said to be perfect. The phase-matching conditions arise from the fact that the OPDC process is a coherent process in which all parts of the crystal contribute in phase. For finite L the wave-number phase-matching condition is relaxed so that $|\Delta|$ may vary over an interval of order $1/L$.

The state $|\Psi\rangle$ is a linear superposition of the vacuum state and a state containing two photons. In general, the second term is much smaller than the first by 5–6 orders of magnitude. Higher-order terms containing four, six, etc. photons are negligible for continuous pumping with power below 1 W. The two-photon part of the state is an entangled state in frequency and wave number, but is not entangled in polarization. In frequency space, the entanglement is a result of the frequency phase-matching condition, which implies that the detection of a photon at frequency ω requires the other photon to have the frequency $\omega_p-\omega$. This is the origin of interesting experiments aimed at illuminating the Einstein-Podolsky-Rosen paradox. The frequency correlation has interesting consequences for the temporal behavior of the photon pair, as we shall see. The state is also entangled with respect to the wave number since the function h defined in (8) cannot be written as a product of a function of k times a function of k'. In the general noncollinear case, the wave-number entanglement has implications for the spatial correlations of the photon pair [12]. In the collinear case, the spatial and temporal correlations are indistinguishable. The lack of entanglement in polarization is a special feature of the collinear case and follows from the symmetry of the state with respect to the frequency and wave number. If we evaluate the two-photon state in the coordinate representation we find

$$\Phi=|o\rangle|e\rangle F(z,z')=|o\rangle|e\rangle\sum_{k,k'}F_{kk'}\frac{1}{2\pi\hbar}e^{i(kz+k'z')}\ .$$

It is only in the collinear case that the polarization states can be factored out because the polarization vectors are the same for all the k's.

III. THE TWO-PHOTON WAVE FUNCTION

In most experiments the two-photon correlation is the quantity of primary interest. For completeness, the single-photon wave function is discussed in Appendix B. In order to measure the two-photon correlation consider the simplified experiment shown in Fig. 1. The beam splitter is assumed to be polarization dependent so that the o ray is transmitted and the e ray is reflected.

The average coincidence counting rate is defined by

$$R_c=\lim_{T\to\infty}\frac{1}{T}\int_0^T dT_1\int_0^T dT_2\langle\Psi|E_1^{(-)}E_2^{(-)}E_2^{(+)}E_1^{(+)}|\Psi\rangle \times S(T_1-T_2)\ , \tag{10}$$

where the electric fields are defined in free space in analogy with Eq. (2). The subscripts $j=1,2$ mean that the field is evaluated at the detector j at time T_j. $S(t)$ is the coincidence window function, which is defined so that $S=1$ for $|t|<t_{\rm coin}$ and goes to zero rapidly for $|t|>t_{\rm coin}$. In the experiments discussed below $t_{\rm coin}$ is large and so we may take $S=1$. It is most convenient to perform the calculations in the Heisenberg picture in which the state vector is the steady-state output at the face of the crystal.

With Ψ given by (6), it is easy to see that

$$\langle\Psi|E_1^{(-)}E_2^{(-)}E_2^{(+)}E_1^{(+)}|\Psi\rangle=|\langle 0|E_2^{(+)}E_1^{(+)}|\Psi\rangle|^2 =|A(t_1,t_2)|^2\ , \tag{11}$$

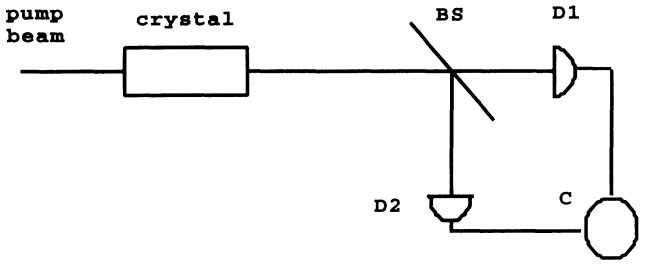

FIG. 1. A birefringent crystal converts the pump beam into a pair of collinear down-converted beams. BS is a polarization-dependent beam splitter which transmits the o ray and reflects the e ray, $D1$ and $D2$ are photodetectors, and C is the coincidence counter.

where $t_r = T_r - s/c$ and s is the optical path length from the surface of the crystal to the r detector $r=1,2$. We take $s_1 = s_2 = s$ to simplify the discussion. The function $A(t_1,t_2)$ is referred to as the *two-photon amplitude,* or for short the *biphoton* [12].

Suppose that for the collinear case, we have perfect phase matching at the angular frequencies Ω_o and Ω_e. It is shown in detail in Appendix C that

$$A(t_1,t_2) = v(t_1+t_2)u(t_1-t_2) , \tag{12}$$

$$u(t) = e^{-i\omega_d(t/2)}\Pi(t) , \tag{13}$$

and

$$v(t) = v_0 e^{-i\omega_p(t/2)} , \tag{14}$$

where $\omega_d = \Omega_o - \Omega_e$. All the slowly varying quantities and constants have been absorbed into v_0. The function $\Pi(t)$, illustrated in Fig. 2, is the rectangular function defined by

$$\Pi(t) = \frac{1}{2\pi}\int_{-\infty}^{\infty} d\nu\, h(-\nu DL)e^{-i\nu t} = \begin{cases} \dfrac{1}{DL} , & DL > t > 0 \\ 0 \text{ otherwise} , \end{cases} \tag{15}$$

where

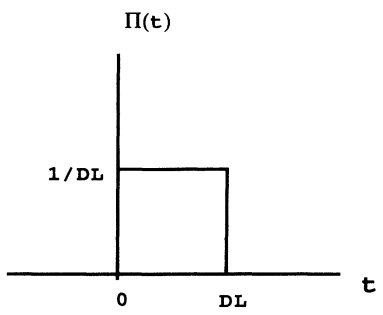

FIG. 2. Plot of $\Pi(t)$ for the case $D>0$.

$$D = \frac{1}{u_o} - \frac{1}{u_e} \tag{16}$$

is the difference between the inverse group velocities of the o and e rays at the frequencies Ω_e and Ω_o, respectively. DL is the difference in the time needed for an o-ray and e-ray wave packet to cross the crystal. A typical value for a beta barium borate (BBO) crystal is $D \approx 0.2$ psec/mm.

It is not difficult to understand the physics of (12). Because the two-photon state is entangled, the biphoton does not factor into a function of t_1 times a function of t_2. The factor v describes the fact that the pair can be created at any time. If the pump beam were taken to be a wave packet rather than a plane wave, this term would also become a wave packet with the coherence length of the pump with the consequence that there would be a distribution of pump frequencies and wave numbers. Since $u(t)$ is nonzero only for positive t when $D>0$, the o ray arrives at the first detector after the e ray arrives at the second detector, $t_1 > t_2$. This may be understood with the help of the Feynman diagram in Fig. 3. The pair is created at the same time and at the same point inside the crystal. The wave packets travel through the crystal at u_o and u_e. For $D>0$, the e-polarized photon exits the crystal first and, since the detectors are at an equal distance from the crystal, reaches the detector first.

The experimental verification of the form (15) is reviewed in Sec. V A.

The discussion so far has emphasized the natural bandwidths of the output beams. In most experiments narrow-band frequency filters are placed in front of the detectors. To take this into account, the fields (11) must be written as

$$E_j^{(+)} = \sum_{\mathbf{k}} f_j(\omega_{\mathbf{k}} - \Omega_j)E_{\mathbf{k}} a_{j\mathbf{k}} e^{i(\mathbf{k}\cdot\mathbf{r}-\omega_{\mathbf{k}}t)} , \tag{17}$$

where the filters are peaked at Ω_j, $j=1,2$ and $E_{\mathbf{k}}$ is defined by (2) with the index of refraction equal to one. Referring to the calculation in Appendix C, we can still write Eqs. (11)–(13) with the replacement of $\Pi(t)$ by $\Pi_f(t)$ where

$$\Pi_f(t) = \frac{1}{2\pi}\int_{-\infty}^{\infty} d\nu f_1(\nu)f_2(\nu)h(-\nu DL)e^{-i\nu t} . \tag{18}$$

Except for the narrowest bandwidths (of order 1 nm), the

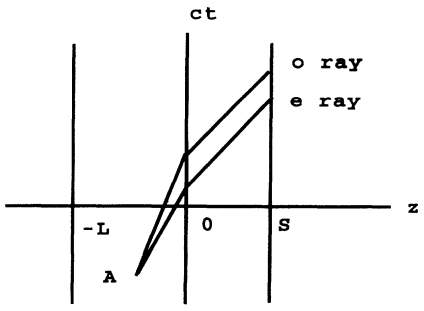

FIG. 3. The photon pair is created at A inside the crystal $(-L<z<0)$. The rays exits the crystal at $z=0$. The case that $u_e > u_o$ $(D>0)$ is illustrated.

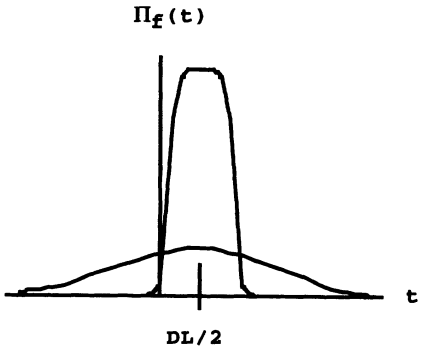

FIG. 4. Sketch of the function $\Pi_f(t)$ for two values of the filter bandwidth σ_0. As σ_0 increases, the natural width DL becomes the dominant factor and the shape becomes more rectangular.

filters may be taken to be Gaussian. Then

$$\bar{f}(\nu)=f_1(\nu)f_2(\nu)=f_0 e^{-\nu^2/\sigma_0^2}, \tag{19}$$

where

$$\frac{1}{\sigma_0^2}=\frac{1}{2\sigma_1^2}+\frac{1}{2\sigma_2^2} \tag{20}$$

and σ_j is bandwidth f_j. Using (19), the integral in (18) can be evaluated in terms of error functions

$$\Pi_f(t)=f_0\{\mathrm{erf}(\sigma_0 t/2)-\mathrm{erf}[(\sigma_0 t-DL)/2]\}/2DL . \tag{21}$$

This function, which is sketched in Fig. 4, peaks at $t=DL/2$ and has a width on the order of $DL+8/\sigma_0$. If we take $L=0.5$ nm, $D=0.2$ psec/nm and convert the bandwidth in angular frequency σ_0 to the full width at half maximum (FWHM) in wavelength in nanometers, $\Delta\lambda$, we get $\sigma_0 DL\approx\Delta\lambda/4$. Thus, if $\Delta\lambda\gg 16$ nm, the shape of Π_f becomes approximately the same as the Π. In the opposite case of a narrow filter, $\Delta\lambda\ll 16$ nm, the shape of the biphoton is determined by the filter. Note that the result is unchanged if only a single filter of bandwidth σ_0 is used.

IV. LINEAR OPTICAL TRANSFORMATION OF THE BIPHOTON

Experimental studies using OPDC require the manipulation of the beams using linear optical devices (see Fig. 5). In the case of type-II OPDC these include phase plates, polarizers, and beam splitters. In order to treat these systematically, it is convenient to use the Heisenberg picture and include them in the detector fields. In all the experiments discussed below the beam splitters are not polarization dependent and have equal transmission and reflection coefficients. Suppose that there are polarizers in front of the detectors. Let $\hat{\mathbf{e}}_1$ and $\hat{\mathbf{e}}_2$ be the polarization vector transmitted through the analyzers in front of detectors 1 and 2, respectively, and let $\hat{\mathbf{e}}_1'$ and $\hat{\mathbf{e}}_2'$ be the orthogonal polarization vectors.

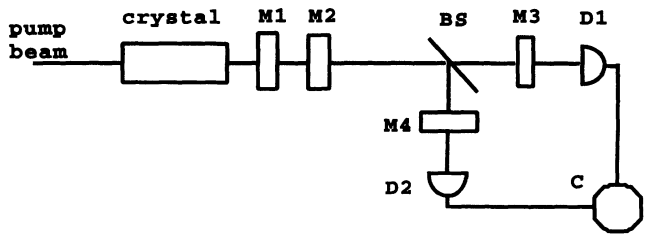

FIG. 5. The transformation of the beam by linear optical elements. BS ia a 50-50 polarization-independent beam splitter.

The linear transformation between the input and detected destruction operators may be written as

$$\begin{bmatrix} a_{jk} \\ 0 \end{bmatrix}=\mathbf{D}^{(j)}(k)\begin{bmatrix} a_{ok} \\ a_{ek} \end{bmatrix}, \quad j=1,2 . \tag{22}$$

If this is substituted into the free fields, for detector j, we get

$$E_j^{(+)}=\sum_k E_{jk}[\mathbf{D}_{1o}^{(j)}(k)a_{0k}+\mathbf{D}_{1e}^{(j)}(k)a_{ek}]e^{-i\omega_{jk}(T-s/c)}, \tag{23}$$

where the matrix elements are labeled by the detector number and the polarization index at the crystal. It will be convenient to replace the k dependence in $\mathbf{D}$ by $(i/c)d/dT$.

In general, $\mathbf{D}$ will be a product of the matrices of several devices so that $\mathbf{D}=\mathbf{M}_n,\ldots,\mathbf{M}_1$, where the $\mathbf{M}$ matrices connect the input and output polarizations of the devices as shown in Fig. 5.

For example, if $\mathbf{D}$ is independent of $\mathbf{k}$,

$$A(t_1,t_2)=v(t_1+t_2)\{D_{1o}^{(1)}D_{1e}^{(2)}u(t_1-t_2)+D_{1e}^{(1)}D_{1o}^{(2)}u(-t_1+t_2)\} . \tag{24}$$

The form of (24) shows that the polarization part of the wave function is entangled by the beam splitter and the detection scheme. This may be seen as follows. The beam splitter allows each polarized beam to be transmitted or reflected. This means that $|o\rangle|e\rangle \rightarrow(|o\rangle_1+|o\rangle_2)(|e\rangle_1+|e\rangle_2)/2$, where 1 and 2 refer to the transmitted and reflected beams. The polarizers in front of the detectors convert this state into the product state $(|\mathbf{e}_1,o\rangle_1+|\mathbf{e}_2,o\rangle_2)(|\mathbf{e}_1,e\rangle_1+|\mathbf{e}_2,e\rangle_2)/2$. The detection scheme projects only the cases in which one photon goes to each detector and so finally we have the entangled state $(|\mathbf{e}_1,o\rangle_1|\mathbf{e}_2,e\rangle_2+|\mathbf{e}_2,o\rangle_2|\mathbf{e}_1,e\rangle_1)/2$.

As a second example, we consider the case in which $M1$ in Fig. 5 is a phase plate oriented so that its fast and slow axes are parallel to the o axis and e axis. In this case, $\mathbf{D}^{(j)}(\phi,k)=\mathbf{R}^{(j)}(\phi)\mathbf{P}(k)$, where the phase plate matrix is written as

$$\mathbf{P}(k)=e^{i(kZ/2)}\begin{bmatrix} e^{-i(k\zeta/2)} & 0 \\ 0 & e^{i(k\zeta/2)} \end{bmatrix}, \tag{25}$$

where $(Z-\zeta)/2$ and $(Z+\zeta)/2$ are the optical path lengths of, respectively, the o-polarized input beam and the e-polarized input beam in the phase plate. $\mathbf{R}^{(j)}(\phi)$ is a

two-dimensional rotation matrix that rotates the output axes of $\mathbf{P}$ into the axes of the analyzer $\hat{\mathbf{e}}_j$ and $\hat{\mathbf{e}}'_j$. Let the detector polarizers make angles ϕ_1 and ϕ_2 relative to the output axes of the phase plate; then

$$\mathbf{D}^{(1)}(\phi_1,k)=e^{i(kZ/2}\begin{bmatrix} e^{-i(k\xi/2)}\cos\phi_1 & -e^{i(k\xi/2)}\sin\phi_1 \\ e^{-i(k\xi/2)}\sin\phi_1 & e^{i(k\xi/2)}\cos\phi_1 \end{bmatrix} \tag{26a}$$

and

$$\mathbf{D}^{(2)}(\phi_2,k)e^{i(kZ/2)}\begin{bmatrix} -e^{-i(k\xi/2)}\cos\phi_2 & e^{i(k\xi/2)}\sin\phi_2 \\ e^{-i(k\xi/2)}\sin\phi_2 & e^{i(k\xi/2)}\cos\phi_2 \end{bmatrix} . \tag{26b}$$

The minus sign in the first column of (26b) is required so that the coordinate system for the reflected beam is right handed. In this case,

$$\begin{aligned} A(t_1,t_2)=\Big\{&\mathbf{D}^{(1)}_{1o}\left[\phi_1,\frac{id}{cdt_1}\right]\mathbf{D}^{(2)}1e\left[\phi_2,\frac{id}{cdt_2}\right] \\ &\times v(t_1+t_2)u(t_1-t_2) \\ &+\mathbf{D}^{(2)}_{1e}\left[\phi_2,\frac{id}{cdt_1}\right]\mathbf{D}^{(1)}_{1o}\left[\phi_1,\frac{id}{cdt_2}\right] \\ &\times v(t_1+t_2)u(-t_1+t_2)\Big\} \end{aligned} \tag{27}$$

or, introducing $\mathbf{d}^{(j)}(\phi)=\mathbf{D}^{(j)}(\phi,0)$,

$$\begin{aligned} A(t_1,t_2)=v&\left[t_1+t_2-\frac{Z}{c}\right] \\ &\times\left\{\mathbf{d}^{(1)}_{1o}(\phi_1)\mathbf{d}^{(2)}_{1e}(\phi_2)u\left[t_1-t_2+\frac{\xi}{c}\right]\right. \\ &\left.+\mathbf{d}^{(2)}_{1o}(\phi_2)\mathbf{d}^{(1)}_{1e}(\phi_1)u\left[-t_1+t_2+\frac{\xi}{c}\right]\right\} . \end{aligned} \tag{28}$$

If ξ is positive, then the e ray travels along the slow axis of the phase plate and is delayed relative to the o ray. In the first term in large curly brackets the o ray goes to detector 1. The center of the biphoton is shifted from $t_1-t_2=DL/2$ to the earlier relative time $DL/2-\xi/c$. In the second term where the o ray goes to detector 2, the center is shifted from $t_1-t_2=-DL/2$ to the later relative time $-DL/2+\xi/c$. If we choose $\xi=DLc/2$, the two terms completely overlap in time.

V. REVIEW OF THE EXPERIMENTS

A. Experimental verification of the Π shape of the biphoton and two-photon anticorrelation

We consider collinear degenerate beams passing through a system like the one illustrated in Fig. 5. The only optical element is $M1$, a phase plate oriented parallel to the o and e axes. Equation (A15) may be written as

$$\begin{aligned} A(t_1,t_2)=&\tfrac{1}{2}v(t_1+t_2-T) \\ &\times\{\cos\phi_1\sin\phi_2 u(t_1-t_2+\tau) \\ &-\cos\phi_2\sin\phi_1 u(-t_1+t_2+\tau)\} . \end{aligned} \tag{29}$$

In this expression $T=Z/c$ and $\tau=\xi/c$, where Z and ξ are defined following Eq. (28). Setting $\phi_1=\phi_2=\pi/4$, the counting rate becomes

$$R_c(\tau)=2R_0[1-\rho(2\tau)/2] , \tag{30}$$

where

$$R_0=N\int_{-\infty}^{\infty}dt\,|u(t)|^2 , \tag{31}$$

$$\begin{aligned} \rho(T)&=2N\int_{-\infty}^{\infty}dt\ \mathrm{Re}[u(t-T)u(-t)]/R_0 \\ &=2\int_{-\infty}^{\infty}dt\ \Pi(t-T)\Pi(-t)\Big/\int_{-\infty}^{\infty}dt\,|\Pi(t)|^2 . \end{aligned} \tag{32}$$

N is an overall constant that is related to the absolute coincidence counting rate. When $\tau=0$, $\rho=0$ since there is no temporal overlap of the two parts of the biphoton $\Pi(t)$ and $\Pi(-t)$. The counting rate vanishes when $\tau=DL/2$ and $\rho(2\tau)=2$. In this case the two parts of the biphoton are overlapped completely. As τ is varied the shape of $\rho(2\tau)$ is a triangular-shaped notch. This is shown in Fig. 6, taken from the experiment reported in [14]. In this experiment, since BBO is a negative uniaxial crystal $D>0$, $M1$ is composed of a number of quartz phase plates oriented so that they introduce a phase delay in the e ray relative to the o ray by the amount $(n_{qe}-n_{qo})L_q/c$, where the q subscript indicates the quartz. L_q is varied by varying the number of plates. When the delay equals $DL/2$ we get complete overlap and zero counting rate. Note that it is the difference in the inverse of the phase velocities that appears here, while inside the down-conversion cyrstal it is the difference in the inverse of the group velocity that occurs. The reason for this is that the phase-matching condition inside the crystal causes the term containing the inverse of the phase velocities to vanish.

If we now insert filters in front of the detectors, then in Eq. (32) we replace Π by Π_f. The experimental result is shown in Fig. 7 from [15].

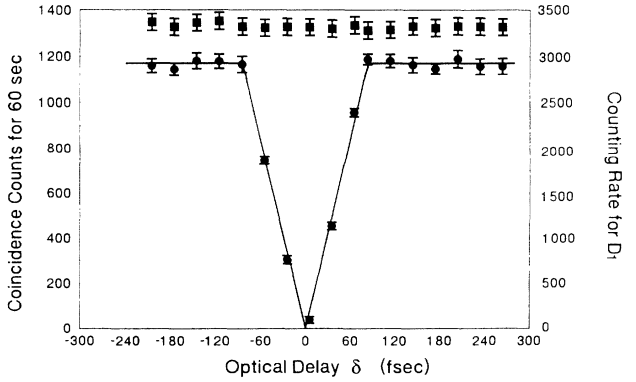

FIG. 6. The solid line is a theoretical fit to the data for the coincidence counting rates reported in [14]. The upper data are the counting rate for a single detector, which is simply constant.

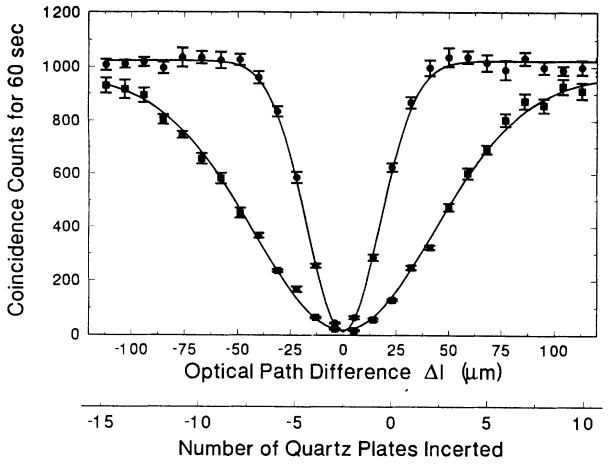

FIG. 7. The coincidence counting rate for two sets of filters with FWHMS of 3.4 and 9.0 nm. The solid curves are Gaussian fits.

B. Two-photon entanglement in type-II OPDC

The experimental setup is the same as in Sec. V A with the phase shifter M_1 set so that we get complete overlap of the two parts of the biphoton (the $\rho=2$ case). In this case, because the two terms in (29) have the same spatial form, we can think of the state of system after leaving the phase plate $M1$ as having the polarization wave function

$$|\Psi\rangle=|o\rangle|e\rangle \ . \tag{33}$$

Suppose a quarter wave plate rotated through an angle Ψ is now inserted into the beam to convert the beams from linear to elliptically polarized beams ($M2$ in Fig. 5). In the notation of (26)

$$\mathbf{D}^{(j)}(\phi_j,k)=\mathbf{R}^{(j)}(\phi_j)\mathbf{P}(k)\mathbf{R}(\Psi) \ , \tag{34}$$

where $\mathbf{R}(\Psi)$ is the two-dimensional rotation that rotates the o-e axes into the fast and slow axes of the quarter wave plate and $\mathbf{P}(k)$ and $\mathbf{R}^{(j)}(\phi_j)$ are defined in Sec. IV. The angles ϕ_1 and ϕ_2 are defined with respect to the axes of the quarter wave plate. We can ignore the part of the wave function corresponding to both photons going to one detector since we project those terms to zero with our detection scheme. For a quarter wave plate we take $k\zeta/2=\pi/4$ independent of k; then

$$R_c=R_0\{\sin^2(\phi_1-\phi_2)\cos^2(2\Psi) + \cos_2(\phi_1+\phi_2)\sin_2(2\Psi)\} \ . \tag{35}$$

If $\Psi\equiv 0$, the o polarization and e polarization are phase shifted relative to one another. This phase shift is small and does not affect the counting rate and we get the result

$$R_c=r_0\sin^2(\phi_1-\phi_2) \tag{36}$$

for the coincidence of two linearly polarized rays. If $\Psi=\pi/4$, Eq. (35) becomes

$$R_c=R_0\cos^2(\phi_1+\phi_2) \ , \tag{37}$$

which is the coincidence rate for a state with polarization

$$|\Phi'\rangle=\tfrac{1}{2}(|R\rangle_1|R\rangle_2+|L\rangle_1|L\rangle_2) \ . \tag{38}$$

To see this, start wtih the polarization state (33), which the quarter wave plate transforms into the state

$$|\Phi\rangle=(i|s\rangle\sin\Psi+|f\rangle\cos\Psi)(-i|s\rangle\cos\Psi+|f\rangle\sin\Psi) \ , \tag{39}$$

where $|s\rangle$ and $|f\rangle$ are the states with polarization along the slow and fast axes of the quarter wave plate. At the beam splitter [16]

$$\begin{aligned} |s\rangle &\rightarrow \frac{1}{\sqrt{2}}(|s\rangle_1+|s\rangle_2) \ , \\ |f\rangle &\rightarrow \frac{1}{\sqrt{2}}(|f\rangle_1-|f\rangle_2) \ , \end{aligned} \tag{40}$$

where the subscripts refer to the transmitted and reflected beams. Substituting these expressions into (39) leads to the state

$$\begin{aligned} |\Phi'\rangle=&(|s\rangle_1|s\rangle_2-|f\rangle_1|f\rangle_2)\tfrac{1}{2}\sin 2\Psi \\ &+(|s\rangle_1|f\rangle_2-|f\rangle_1|s\rangle_2)i\tfrac{1}{2}\cos 2\Psi \ . \end{aligned} \tag{41}$$

For $\Psi=\pi/4$, we get (38) by introducing the right- and left-hand polarized states. More generally we can project (41) onto the detector states with the analyzers $\hat{\mathbf{e}}_1$ and $\hat{\mathbf{e}}_2$ to get the counting rate (35).

Figure 8 shows data from the experiment reported in Ref. [17]. The data are consistent with Eq. (37).

Using Eq. (41), it is easy to see that $|\Phi'\rangle$ is a product state when $\Psi=\pi/8$; otherwise it is an entangled state. It is an EPR state if $\Psi=0$ or $\pi/4$ and is a linear superposition of two EPR states for all other Ψ's ($0\le\Psi<\pi/2$).

C. Two-photon quantum beats between orthogonally polarized photons

We now consider collinear nondegenerate beams passing through a system like the one illustrated in Fig. 5.

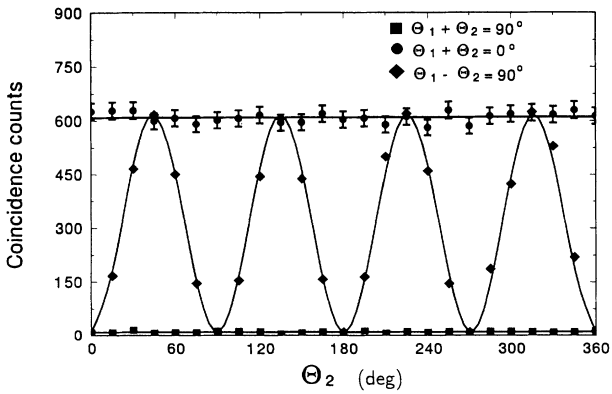

FIG. 8. The coincidence counting rate for the case $\Psi=\pi/4$. If the sum of the angles is fixed at 90° or 0°, there is a zero or a maximum in the counting rate. If the difference between the angles is fixed at 90°, there is a sinusoidal oscillation with a period of $\pi/2$ and 100% visibility.

$M1$ is a phase plate oriented parallel to the o and e axes. $M3$ is a filter whose bandpass is centered at λ_1 and $M4$ is a filter centered at λ_2. The widths of the filters are chosen so that the overlap of their spectral ranges is negligible; therefore, we may assume that only one wavelength reaches each detector. The crystal is oriented so that for that perfect phase matching is satisfied approximately for pairs $(\lambda_1,o;\lambda_2 e)$ and $(\lambda_2,o;\lambda_i,e)$. The analyzers in front of the detectors are oriented at an angles ϕ_1 and ϕ_2 relative to the o axis. The calculation of $A(t_1,t_2)$ is discussed in Appendix C 3. Equation (A15) may be written as

$$A(t_1,t_2)=\tfrac{1}{2}v(t_1+t_2-T) \times\{\cos\phi_1\sin\phi_2 u(t_1-t_2+\tau) -\cos\phi_2\sin\phi_1 u^*(-t_1+t_2+\tau)\}\ . \quad (42)$$

In this expression $T=Z/c$ and $\tau=\zeta/c$, where Z and ζ are defined following Eq. (28). When ζ is small compared to the length of the wave packet, and $\phi_1=\phi_2=\pi/4$, the counting rate is given by

$$R_c\approx R_0\sin^2\left[\frac{\omega_d(\tau-\tau_0)}{2}\right] \quad (43)$$

with $\omega_d=2\pi c(1/\lambda_1-1/\lambda_2)$ and $\tau_0=DL/2$. The minimum occurs when the two terms in curly brackets in (42) completely overlap, which is when $\tau=\tau_0$: recall that τ_0 is the average of the time difference it takes o-ray and e-ray wave packets to cross the crystal.

The state generating the amplitude (42) is entangled jointly in polarization and wavelength. In a simplified picture, we have, for the wave function just before it enters the beam splitter,

$$e^{i\omega_d(\tau-\tau_0)/2}|\lambda_1,o\rangle|\lambda_2,e\rangle+e^{-i\omega_d(\tau-\tau_0)/2}|\lambda_1,e\rangle|\lambda_2,o\rangle\ ,$$

where the phase is the result of the relative delay due to the phase plates in the o and e-ray rays. The joint entanglement is crucial to the interference between the two amplitudes.

The delay τ is varied by changing the length of the phase plate in the manner described above in Sec. V A. Data are shown in Fig. 9 from the experiment reported in [18].

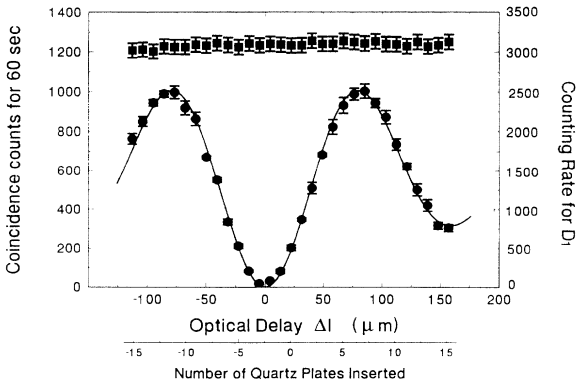

FIG. 9. Difference frequency oscillations with 100% visibility showing the biphoton quantum beats between orthogonally polarized photons.

Finally we note that the single-detector counting rate shows no modulation when either the polarizer in front of the detector is rotated or there is a change in the relative time delay of the two polarization beams. This is shown in the upper part of Fig. 9. In Eq. (42), if we keep τ fixed and vary the orientation of the polarizers, then we get interference effects similar to those discussed in Sec. V A. This demonstrates both space-time and spin entanglement in one experimental configuration. It is only in the collinear case that the states $|o\rangle$ and $|e\rangle$ are independent of $\mathbf{k}$.

D. A different type of second-order interferometer

We have discussed the theory and the experimental observations of two-photon polarization correlation, two-photon anti-correlation, and two-photon quantum beating. These are all examples of biphoton interference effects. In this section we discuss another type of two-photon interference in which the oscillation is at the sum frequency ω_p, the pump frequency.

Two types of experiments have been reported that show this effect. In the first type [19–21], each member of the photon pair is first sent through a balanced mach-Zehnder interferometer before entering an unbalance interferometer. The first interferometer causes both photons to traverse either the long or the short path through the second interferometer. In the second type of experiment [22–26] each member of the photon pair is sent through an interferometer with a long and short path, denoted by L and S, respectively. The biphoton can then be written schematically as $A(L,L)+A(L,S)+A(S,L)+A(S,S)$. In order to see the quantum interference (visibilities greater than 50%) it is necessary to cutoff the middle two terms. This is by using the coincidence window. As we shall see, for the experiment described below, the cancellation of the unwanted amplitudes is effected by exploiting the polarization entanglement to see the quantum space-time interference.

The experimental setup is illustrated in Fig. 10. The down-conversion is nondegenerate and the filters $F1$ and $F2$ are chosen to have wide bandwidths so that both frequencies can reach each detector. Following the down-conversion crystal a set of quartz phase plates $M1$ is inserted, which introduces a phase delay in the e ray relative to the o ray by the amount $(n_{qe}-n_{qo})L_q/c=DL/2$, where the q subscript indicates the quartz. This gives us complete overlap between the two parts of the biphoton

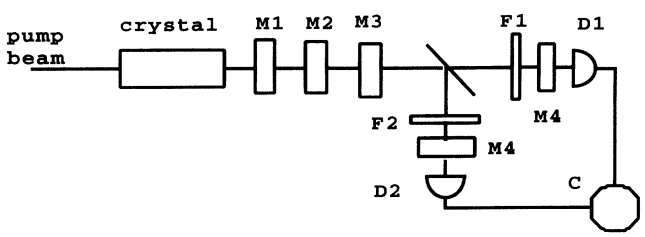

FIG. 10. Different type of interferometer.

$\Pi(t)$ and $\Pi(-t)$. Another set of quartz phase plates $M2$ is oriented at 45° relative to the o and e axes of the crystal. The length of these is long enough so that the emerging beams polarized along the x' and y' axes *do not* overlap. The optical delay between them is much greater than the single-photon coherence length. $M3$ is a Pockel cell with the same orientation as $M2$, which is used to provide a fine variation in the relative optical path length of the two polarizations. The analyzers in front of the detectors are oriented at 0° relative to the initial x axis.

For the case in which the angle of rotation of the $M2$ is Ψ, we write the first row of the transformation matrices

$$\mathbf{D}_{1*}^{(1)}(0,k)=e^{i\omega(\tau_o+\tau_x')}[\cos^2\Psi+e^{-i\omega\Delta\tau'}\sin^2\Psi\ ,e^{i\omega\Delta\tau}(1-e^{-i\omega\Delta\tau'})\sin\Psi\cos\Psi]\ ,$$
$$\mathbf{D}_{1*}^{(2)}(0,k)=e^{i\omega(\tau_o+\tau_x')}[e^{i\omega\Delta\tau}(\sin^2\Psi+e^{-i\omega\Delta\tau'}\cos^2\Psi)\ ,(1-e^{-i\omega\Delta\tau'})\sin\Psi\cos\Psi]\ , \tag{44}$$

where $k=\omega/c$ and τ_o and $\tau_{x'}$ are the optical path length through $M1$ and $M2$ along the o and x' axes, respectively. The difference in optical path lengths along the e and o axes in $M1$ is $\Delta\tau$ and along the x' and y' axes in $M2$ is $\Delta\tau'$. Using this result, it is not too difficult to show that

$$A(t_1,t_2)=W\cos\Psi\sin\Psi\{[v(\tau_1+\tau_2-\Delta\tau)\cos^2\Psi-v(\tau_1+\tau_2-\Delta\tau+2\Delta\tau')\sin^2\Psi]u(\tau_1-\tau_2+\Delta\tau)$$
$$+v(\tau_1+\tau_2-\Delta\tau+\Delta\tau')[-\cos^2\Psi u(\tau_1-\tau_2+\Delta\tau-\Delta\tau')+\sin^2\Psi]u(\tau_1-\tau_2+\Delta\tau+\Delta\tau')]\}+(t_1\rightleftarrows t_2)\ , \tag{45}$$

where W is a slowly varying quantity which need not concern us. We have defined $\tau_1=t_1-(\tau_o+\tau_{x'})$ and $\tau_2=t_2-(\tau_o+\tau_{x'})$.

The expression in (45) contains four amplitudes. The first term corresponds to the case that o- and e-polarized photons both passing along the x' axis of $M2$. The second term corresponds to both photons traveling along the y' axis of $M2$. The third term corresponds to the o photon traveling along the x' axis and the e photon along the y' axis of $M3$ and the fourth term is the reverse case. In all these terms the x photon is detected at $D1$ and the y photon at $D2$. The terms obtained by interchanging t_1 and t_2 corresponds to the x photon being detected at $D2$ and the y photon at $D1$.

We now set $\Psi=45°$ and let $\Delta\tau=DL/2$ so that $u(t+\Delta\tau)=u(-t+\Delta\tau)$. In (45) only the first term and its partner obtained by interchanging t_1 and t_2 survive. The other terms cancel exactly, independent of the delay $\Delta\tau'$ because the terms shown in (45) are out of phase with those obtained by interchanging t_1 and t_2. Then, using

$$v(t+\Delta\tau')=e^{-i\omega_p\Delta\tau'}v(t) \tag{46}$$

reduces

$$A(t_1,t_2)=\frac{W}{4}v(\tau_1+\tau_2-\Delta\tau)(1-e^{-i\omega_p\Delta\tau'})$$
$$\times\{u(\tau_1-\tau_2-\Delta\tau)+u(-\tau_1+\tau_2-\Delta\tau)\} \tag{47}$$

and the counting rate becomes

$$R_c=R_0(1-\cos\omega_p\Delta\tau')\ . \tag{48}$$

By varying the voltage on the Pockel cell, $\Delta\tau'$ may be varied and the counting rate oscillates at the pump frequency with 100% visibility. This is shown in Fig. 11 [27].

The terms in the complicated expression (45) can be derived easily using the Schrödinger-like picture discussed above. Since both detectors can detect both photons we take them to be of the same frequency in this simplified model. After leaving $M1$ the polarization state can be written in the form (33). The phase plate transforms this state into an expression like (39), except the factor i is replaced by $\exp(i\omega_p\Delta\tau'/2)$ and we take $\Psi=\pi/4$ for simplicity. Then after the beam splitter transformation (40) we have

$$|\Phi'\rangle=(e^{i\omega_p\Delta\tau'}|s\rangle_1|s\rangle_2-|f\rangle_1|f\rangle_2)\frac{1}{2\sqrt{2}}$$
$$+e^{i(\omega_p/2)\Delta\tau'}(|s\rangle_1|f\rangle_2-|f\rangle_1|s\rangle_2)\frac{1}{2\sqrt{2}}\ , \tag{49}$$

where we retain only the terms that the coincidence counter detects. Projecting these states onto the detector analyzer states we get

$$\tfrac{1}{4}|o\rangle_1|o\rangle_2(-1+e^{i\omega_p\Delta\tau})\ . \tag{50}$$

The second term cancels exactly. This simple picture

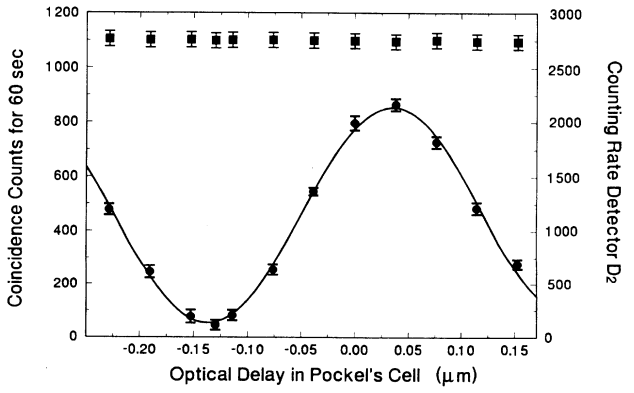

FIG. 11 Sum frequency oscillation for the interferometer shown in Fig. 10.

does not fully illustrate the curious nature of this cancellation. Recall that if one tries to envision the wave function in terms of individual photons, the photons that emerge with polarization s have been delayed relative to those with polarization f by an amount exceeding the single-photon coherence length. This is one reason for not relying too heavily on a picture of the biphoton as a pair of single photons.

VI. CONCLUSIONS

We have discussed the nature of the two-photon state or biphoton for type-II optical parametric down-conversion. The nature of the state is such as to allow a number of interesting quantum-mechanical interference experiments to be performed which illustrate the entanglement of spin and space-time variables and the generation of EPR states. In the experiment discussed in Sec. V A the degree of entanglement is determined by the length of the crystal, the dispersion in the crystal, and the bandwidth detected. This dependence is in sharp contrast with the entanglement produced in experiments using type-I down-conversion [28].

In the quantum beating experiment the polarization and space-time entanglement is illustrated in an interesting way. The detectors see nonoverlapping frequency bands. The state produced following the beam splitter is entangled in both space-time (or, equivalently, in frequency and wave number) and in the polarization. The space-time entanglement is illustrated by the beating at the difference frequency. The polarization effects may also be observed by rotating the analyzers at the detectors.

In the final experiment discussed above, it was shown how a different type of interferometer allow us to perform an EPR-type experiment of the type proposed by Franson. However, in this case the creation of the EPR entangled state is realized by the cancellation of amplitudes by the adjustment of polarizers rather than a coincidence time window.

ACKNOWLEDGMENTS

This work was supported by the U.S. Office of Naval Research, Grant No. N00014-91-J-1430. We also wish to thank the National Institute of Standards and Technology and the International Science Foundation for their support of the visit of D.N.K.

APPENDIX A: TYPE-II PARAMETRIC DOWN-CONVERSION

In this appendix we calculate the initial state for type-II down-conversion in the general case. The interaction Hamiltonian is given by Eq. (1) and the electric field of an output beam with polarization j is given by Eq. (2) in the text. In the general case $\mathbf{k}$ does not lie along the z axis and the direction of the polarization vector $\hat{\mathbf{e}}_j$ is determined from the Fresnel equations for uniaxial crystals.

The calculation of the state vector to first order in perturbation theory gives

$$|\Psi\rangle = |0\rangle - \frac{i}{\hbar}\int_{-\infty}^{\infty} dt\, H_1 |0\rangle = |0\rangle + \sum_{\mathbf{k},\mathbf{k}'} F_{\mathbf{k}\mathbf{k}'} a_{o\mathbf{k}}^{\dagger} a_{e\mathbf{k}'}^{\dagger} |0\rangle \ , \tag{A1}$$

where

$$F_{\mathbf{k}\mathbf{k}'} = \Gamma_{\mathbf{k}\mathbf{k}'} \delta(\omega_{o\mathbf{k}} + \omega_{e\mathbf{k}'} - \omega_p) L h(L\Delta_{\mathbf{k}\mathbf{k}'}) h_{\mathrm{tr}}(\mathbf{k},\mathbf{k}') \tag{A2}$$

and

$$\Gamma_{\mathbf{k}\mathbf{k}'} = \frac{-i}{\hbar} E_{o\mathbf{k}} E_{e\mathbf{k}'} 2\pi\varepsilon_0 \chi E_0 A \ . \tag{A3}$$

The z integral from $-L$ to 0 over the length of the crystal gives $Lh(L\Delta_{\mathbf{k}\mathbf{k}'})$, where

$$h(x) = \frac{1 - e^{-ix}}{ix} \tag{A4}$$

and

$$\Delta_{\mathbf{k}\mathbf{k}'} = k_p - k_z - k_z' \ . \tag{A5}$$

The integral over the area A of the intersection of the beam cross section and the crystal gives

$$h_{\mathrm{tr}}(\mathbf{k},\mathbf{k}') = \frac{1}{A}\int_A d^2\rho\, e^{i(\mathbf{k}+\mathbf{k}')\cdot\rho} \ , \tag{A6}$$

where we assume that A is independent of z and tr means transverse. The time integral gives the 2π times the Dirac δ function, which is the steady-state or frequency phase-matching condition.

The function h_{tr} depends on the components of the wave number perpendicular to the z axis. In the limit that the area of the beam is large enough so that diffraction effects may be ignored,

$$h_{\mathrm{tr}}(\mathbf{k},\mathbf{k}') = \delta_{-k_x k_x'} \delta_{-k_y k_y'} \ . \tag{A7}$$

In this approximation, the modes are correlated in pairs. Each o ray with $\mathbf{k} = \mathbf{k}_{\mathrm{tr}} + k_z \hat{\mathbf{e}}_z$ is correlated with an e ray with $\mathbf{k}' = -\mathbf{k}_{\mathrm{tr}} + k_z' \hat{\mathbf{e}}_z$. Using the dispersion relation, k_z can be expressed in terms of $\mathbf{k}_{\mathrm{tr}}$ and the angular frequency ω and k_z' can be expressed in terms of $\mathbf{k}_{\mathrm{tr}}$ and the angular frequency $\omega' = \omega_p - \omega$. In most experiments the range of the transverse component of the wave number is limited by placing pin holes in the beams.

It should be recalled that when the beams exit the crystal, the components of the wave numbers parallel to surface of the crystal are continuous across the interface. If the length of the crystal is infinite, then the integral over z becomes a δ function and we obtain the perfect phase-matching conditions

$$\omega_{ok} + \omega_{ek'} = \omega_p \ , \quad \mathbf{k} + \mathbf{k}' = k_p \hat{\mathbf{e}}_z \ . \tag{A8}$$

When these conditions are satisfied we get a maximum in the intensity of the output beams.

In the collinear case, to a good approximation we can ignore the transverse components of the wave vector. Then the modes may be labeled by the angular frequency and the polarization. $\mathbf{k}_o = k_o \hat{\mathbf{e}}_z$ and $\mathbf{k}_e = k_e \hat{\mathbf{e}}_z$, where $k_o(\omega) = \omega n_o(\omega)/c$ and $k_e(\omega) = \omega n_e(\omega)/c$. We also have $\hat{\mathbf{e}}_o = \hat{\mathbf{e}}_x$ and $\hat{\mathbf{e}}_e = \hat{\mathbf{e}}_y$. For the collinear case we may drop the vector notation for the wave numbers. We then ob-

tain Eq. (6) and the perfect phase-matching condition reduces to (9).

The two-photon state in (A1) is entangled in both $\mathbf{k}$ and spin since the polarization vectors are themselves functions of $\mathbf{k}$ because they must satisfy $\hat{\mathbf{e}}\cdot\mathbf{k}=0$.

APPENDIX B: THE SINGLE-PHOTON COUNTING RATE

To discuss the single-photon properties of the radiation, we consider an experiment like that shown if Fig. 1 with the beam splitter removed. The average counting rate is given by

$$R_1=\lim_{T\to\infty}\frac{1}{T}\int_0^T dt_1\langle\Psi|E_1^{(-)}E_1^{(+)}|\Psi\rangle\ . \tag{B1}$$

Applying the free field E_1, which has the polarization vector $\hat{\mathbf{e}}_1$, to Ψ gives

$$E_1^{(+)}|\Psi\rangle=\sum_{k,k'}e^{-ikc(t-\tau_1)}\times E_k(F_{kk'}\hat{\mathbf{e}}_1\cdot\hat{\mathbf{e}}_o a_{ek'}^\dagger+F_{k'k}\hat{\mathbf{e}}_1\cdot\hat{\mathbf{e}}_{ey}a_{ok'}^\dagger)|0\rangle\ , \tag{B2}$$

where $\tau_1=s/c$, s is the distance from the crystal output face to the detector, and E_k is given by Eq. (3) with unit index of refraction. Inspection of (B2) shows that it is a single-photon state which is a superposition of two independent modes. The first term is polarized along the e axis and the second along the o axis. Note that this is the state of the undetected photon.

Now it is a simple matter to show that

$$\langle\Psi|E_1^{(-)}E_1^{(+)}|\Psi\rangle=\sum_k\frac{V_Q^{1/3}}{2\pi}|g(\omega_k)E_k|^2\times\left[\frac{1}{u_{ek'}}(\hat{\mathbf{e}}_1\cdot\hat{\mathbf{e}}_o)^2+\frac{1}{u_{ok'}}(\hat{\mathbf{e}}_1\cdot\hat{\mathbf{e}}_e)^2\right]\ . \tag{B3}$$

To evaluate the Dirac δ functions in $F_{kk'}$ a summation over a wave number is converted into an angular frequency integral. This is done in the usual way

$$\sum_{k_j}\to\frac{V_Q^{1/3}}{2\pi}\int\frac{dk}{d\omega}d\omega=\frac{V_Q^{1/3}}{2\pi}\int\frac{d\omega}{u_j(\omega)}\ , \tag{B4}$$

where u_j is the group velocity of the j-polarized beam. Equation (B3) is the sum of two independent terms due to the o-polarized and e-polarized photons. There is no interference between these terms because the o and e modes of the beam have no definite relative phase. This means that the beam is unpolarized. For a given orientation of the analyzer, $\hat{\mathbf{e}}_1$, the counting rate, is constant. As the analyzer is rotated the last term in (B3) varies. This variation is determined by the difference is the inverse of group velocities of the two beams.

APPENDIX C: EVALUATION OF THE TWO-PHOTON AMPLITUDE

The two-photon amplitude is defined in Eq. (12) as

$$A(t_1,t_2)=\langle 0|E_2^{(+)}E_1^{(+)}|\Psi\rangle\ . \tag{C1}$$

The fields E_1 and E_2 are fields that are defined outside the crystal and therefore in using the definition (2) we must take the index of refraction to be unity. Since for simplicity we assume the detectors are point detectors, the space-time dependence of the fields, $\mathbf{k}\cdot\mathbf{r}_r-\omega_k T_r$ becomes $\omega_k(T_r-s/c)=\omega_k t_r$, where s is the optical path length from the surface of the crystal to the r detector $r=1,2$. The beam splitter transmits the o ray and reflects the e ray.

1. Detection of the natural bandwidth

In this case there are no filters placed in front of the detectors. Substituting Eq. (2) into (C1) gives

$$A(t_1,t_2)=\sum_{\mathbf{k}_1,\mathbf{k}_2}E_{\mathbf{k}_1}E_{\mathbf{k}_2}e^{-i(\omega_{\mathbf{k}_1}t_1+\omega_{\mathbf{k}_2}t_2)}\langle 0|a_{1\mathbf{k}_1}a_{2\mathbf{k}_2}|\Psi\rangle\ . \tag{C2}$$

The $E_{\mathbf{k}}$ are defined by (3) and are independent of the polarization. Next, using (6) we find

$$\langle 0|a_{1\mathbf{k}_1}a_{2\mathbf{k}_2}|\Psi\rangle=\sum_{k,k'}F_{kk'}\delta_{\mathbf{k}_1\mathbf{k}}\delta_{\mathbf{k}_2\mathbf{k}'}\ . \tag{C3}$$

Substituting this into (C2) and evaluating the summations using the Kronecker δ gives

$$A(t_1,t_2)=\sum_{kk'}W_{kk'}\delta(\omega_{ok}+\omega_{ek'}-\omega_p)\times h(L\Delta_{kk'})e^{-i(\omega_k t_1+\omega_{k'}t_2)}\ . \tag{C4}$$

The functions which vary slowly over the bandwidth of the beams have been absorbed into $W_{kk'}$. Recall that $\Delta_{kk'}=k_p-k-k'$.

Suppose that the crystal is oriented so that the perfect phase-matching conditions (10) can be satisfied by the set Ω_o, Ω_e, K_o, and K_e. The bandwidth of the down-converted beams are such that it is possible to select the frequencies such that $\omega=\Omega_o+\nu$ and $\omega'=\Omega_e+\nu'$, where $|\nu|\ll\Omega_o$ and $|\nu'|\ll\Omega_e=\omega_p-\Omega_o$. The δ function in (C4) requires that $\nu=-\nu'$. Now expand k and k' to first order in ν using the dispersion relations

$$k=K_o+\nu\frac{dK_o}{d\Omega_o}=K_o+\frac{\nu}{u_o} \tag{C5}$$

and

$$k'=K_e+\nu'\frac{dK_e}{d\Omega_e}=K_e-\frac{\nu}{u_e}\ . \tag{C6}$$

Now converting the sums in (C4) into integrals in the standard fashion (see B4) and using

$$\Delta_{kk'}=-\nu\left[\frac{1}{u_o}-\frac{1}{u_e}\right]=-\nu D \tag{C7}$$

gives

$$A(t_1,t_2)=W_{K_xK_y}e^{-i(\omega_p/2)(t_1+t_2)}\times\int_{-\Omega_o}^{\Omega_e}d\nu\,h(-\nu DL)e^{-i(\omega_d/2)(t_1-t_2)}\times e^{-i\nu(t_1-t_2)}. \tag{C8}$$

In this expression we have absorbed all the slowly varying quantities into W and introduced the frequency difference $\omega_d=\Omega_o-\Omega_e$. The limits on the integral may be taken to $\pm\infty$ since the function h is peaked around $\nu=0$ and has a bandwidth of order $1/DL$, which is generally much smaller than Ω_o or Ω_e. The integral in (C8) is the Fourier transform of a phase factor times the sinc function and so gives the rectangular function

$$\Pi(t)=\frac{1}{2\pi}\int_{-\infty}^{\infty}d\nu\,h(-\nu DL)e^{-i\nu t}=\begin{cases}\dfrac{1}{DL}, & DL>t>0\\ 0 \text{ otherwise.}\end{cases} \tag{C9}$$

It is now a simple matter to rewrite (C8) in the form given in (13)–(15).

For some orientations of the crystal it may be possible for more than one pair of photons to satisfy the perfect phase-matching condition. In such a case, we must add terms to (C8) for those cases.

2. Detection with restricted bandwidths

We now consider the case in which there are filters placed in front of the detectors. Equation (C2) becomes

$$A(t_1,t_2)=\sum_{\mathbf{k}_1,\mathbf{k}_2}E_{\mathbf{k}_1}E_{\mathbf{k}_2}f_1f_2e^{-i(\omega_{\mathbf{k}_1}t_1+\omega_{\mathbf{k}_2}t_2)}\times\langle 0|a_{1\mathbf{k}_1}a_{2\mathbf{k}_2}|\Psi\rangle\ , \tag{C10}$$

where, for $j=1,2$ the filter f_j is peaked at Ω_j and

$$f_j=f_j(\omega_{\mathbf{k}_j}-\Omega_j)\ . \tag{C11}$$

For the degenerate case, $\Omega_1=\Omega_2=\omega_p/2$. For the nondegenerate case the choice of filters depends on whether the experiment of interest requires that each filter pass both photons or only one of the pair. In the quantum beat experiment discussed in the paper, the filters are selected so that their spectral bands have negligible overlap.

3. Two-photon quantum beats

In this experiment the crystal is oriented so that perfect phase matching is satisfied approximately for two sets of conditions

$$\Omega_0=\Omega_1\ ,\quad \Omega_e=\Omega_2\ ,\qquad K_{1o}=\frac{\Omega_1 n_o(\Omega_1)}{c}\ ,\quad K_2e=\frac{\Omega_2 n_e(\Omega_2)}{c} \tag{C12a}$$

and

$$\Omega_o=\Omega_2\ ,\quad \Omega_e\Omega_1\ ,\qquad K_{2o}=\frac{\Omega_2 n_o(\Omega_2)}{c}\ ,\quad K_{1e}=\frac{\Omega_1 n_e(\Omega_2)}{c}\ . \tag{C12b}$$

In these cases $k_p-K_{10}-K_{2e}=\delta\neq 0$ and $k_p-K_{1e}-K_{2o}=\delta'\neq 0$. In the experiments described in the text it is possible to select $|\delta|,|\delta'|\ll DL$. In this case the Π functions are simply multipled by an overall phase factor which does not effect the results. Now (C8) has four terms. These can give rise to amplitudes $\{(\Omega_1,o)\to 1,\ (\Omega_2,e)\to 2\}$, $\{(\Omega_1,o)\to 2,\ (\Omega_2,e)\to 1\}$, $\{(\Omega_1,e)\to 1,\ (\Omega_2,o)\to 2\}$, and $\{(\Omega_1,e)\to 2,\ (\Omega_2,o)\to 1\}$. If the filters are chosen so that their overlap is negligible, then the second and fourth terms are negligible. In this case, Eq. (C8) becomes

$$A(t_1,t_2)=e^{-i(\omega_p/2)(t_1+t_2)}e^{-i(\omega_d 2)(t_1-t_2)}\times\{W_{K_{1o}K_{2e}}\hat{\mathbf{e}}_1\cdot\hat{\mathbf{e}}_o\hat{\mathbf{e}}_2\cdot\hat{\mathbf{e}}_e\Pi_f(t_1-t_2)+W_{K_{2o}K_{1e}}\hat{\mathbf{e}}_2\cdot\hat{\mathbf{e}}_0\hat{\mathbf{e}}_1\cdot\hat{\mathbf{e}}_e\Pi_{f'}(-t_1+t_2)\}\ , \tag{C13}$$

where Π_f and $\Pi_{f'}$ depend on D and D', respectively, wtih

$$D=\left[\frac{1}{u_{1o}}-\frac{1}{u_{2e}}\right]\ ,\quad D'=\left[\frac{1}{u_{2o}}-\frac{1}{u_{1e}}\right]\ . \tag{C14}$$

In the experiment discussed in the text the e-polarized beam is phase shifted relative to the o-polarized beam. This can be accounted for by recalling that the o-polarized beam is detected at detector 1 in the first term and at detector 2 in the second term. Therefore, let $t_1\to t_1-(L-\zeta)/2c$ and $t_2\to t_2-(L+\zeta)/2c$ in the first term and $t_1\to t_1-(L+\zeta)/2c$ and $t_2\to t_2-(L-\zeta)/2c$ in the second.

Finally to get Eq. (39), we use the assumptions that

$$W_{K_{1o}K_{2e}}\approx W_{K'_{2o}K'_{12}}\ D\approx D'\ .$$

Then

$$A(t_1,t_2)=W_{K_{2o}K_{1e}}e^{-i(\omega_p/2)(t_1+t_2+L/c)}e^{-i(\omega_d/2)(t_1-t_2)}\times\{\hat{\mathbf{e}}_1\cdot\hat{\mathbf{e}}_o\hat{\mathbf{e}}_2\cdot\hat{\mathbf{e}}_e e^{-i\omega_d(s/c)}\Pi_f(t_1-t_2+s/c)+\hat{\mathbf{e}}_2\cdot\hat{\mathbf{e}}_o\hat{\mathbf{e}}_1\cdot\hat{\mathbf{e}}_e e^{i\omega_d(s/c)}\Pi_f(-t_1+t_2+s/c)\}\ . \tag{C15}$$

[1] E. Schrödinger, Naturwissenschaften **23**, 807 (1935); **23**, 823 (1935); **23**, 844 (1935) [translation in *Quantum Theory of Measurement,* edited by J. A. Wheeler and W. H. Zurek (Princeton University Press, Princeton, 1983)].

[2] A. Einstein, B. Podolsky, and N. Rosen, Phys. Rev. **47**, 777 (1935).

[3] D. Bohm, *Quantum Theory* (Prentice-Hall, Englewood Cliffs, NJ, 1951), p. 614.

[4] J. S. Bell, Phys. **1**, 195 (1964); *Speakable and Unspeakable in Quantum Mechanics* (Cambridge University Press, Cambridge, England, 1987).

[5] J. F. Clauser and A. Shimony, Rep. Prog. Phys. **41**, 1881 (1978).

[6] W. H. Louisell, A. Yariv, and A. E. Siegman, Phys. Rev. **124**, 1646 (1961).

[7] N. Bloembergen, *Nonlinear Optics* (Benjamin, New York, 1965).

[8] D. N. Klyshko and D. P. Krindach, Pis'ma Zh. Eksp. Teor. Fiz. **54**, 697 (1968) [JETP Lett. **27**, 371 (1968)].

[9] B. Ya Zeldovich and D. N. Klyshko, Pis'ma Zh. Eksp. Teor. Fiz. **9**, 69 (1969) [JETP Lett. **9**, 69 (1969)].

[10] B. R. Mollow, Phys. Rev. A **8**, 2684 (1973).

[11] C. L. Tang, in *Quantum Electronics: A Treatise,* edited by H. Rabin and C. L. Tang (Academic, New York, 1975).

[12] D. N. Klyshko, *Photons and Nonlinear Optics* (Gordon and Breach Science, New York, 1988).

[13] D. N. Klyshko, Zh. Eksp. Teor. Fiz. **94**, 82 (1988) [Sov. Phys. JETP **67**, 1131 (1988)].

[14] A. V. Sergienko, Y. H. Shih, and M. H. Rubin (unpublished).

[15] Y. H. Shih and A. V. Sergienko, Phys. Lett. A **186**, 29 (1994).

[16] The minus sign in this transformation is explained following Eq. (27).

[17] Y. H. Shih, A. V. Sergienko, M. H. Rubin, T. E. Kiess, and C. O. Alley, Phys. Rev. A **50**, 23 (1994).

[18] Y. H. Shih and A. V. Sergienko, Phys. Rev. A **50**, 2564 (1994).

[19] J. G. Rarity, P. R. Tapster, E. Jakeman, T. Larchuk, R. A. Campos, M. C. Teich, and B. E. A. Saleh, Phys. Rev. Lett. **65**, 1348 (1990).

[20] Z. Y. Ou, X. Y. Zou, L. J. Wang, and L. Mandel, Phys. Rev. A **42**, 2957 (1990).

[21] T. S. Larchuk, R. A. Campos, J. G. Rarity, P. R. Tapster, E. Jakeman, B. E. A. Saleh, and M. C. Teich, Phys. Rev. Lett. **70**, 1603 (1990).

[22] J. D. Franson, Phys. Rev. Lett. **62**, 2205 (1989).

[23] J. Brendel, E. Mohler, and W. Martienssen, Phys. Rev. Lett. **66**, 1142 (1993).

[24] P. G. Kwait, A. M. Steinberg, and R. Y. Chiao, Phys. Rev. A **47**, 2472 (1993).

[25] Y. H. Shih, A. V. Sergienko, and M. H. Rubin, Phys. Rev. A **47**, 1288 (1993).

[26] Two pioneering experiments of this type, which did not have visibilities greater than 50% because their coincident time windows did not cut off the *LS* and *SL* amplitudes, are by Z. Y. Ou, X. Y. Zou, L. J. Wang, and L. Mandel, Phys. Rev. Lett. **65**, 321 (1990); P. G. Kwait, W. A . Vareka, C. K. Hong, H. Nathel, and R. Y. Chiao, Phys. Rev. A **41**, 2910 (1990).

[27] Y. H. Shih and A. V. Sergienko, Phys. Lett. A **191**, 201 (1994).

[28] T. E. Kiess, Y. H. Shih, A. V. Sergienko, and C. O. Alley, Phys. Rev. Lett. **71**, 3893 (1993).